DANISH METEOROLOGICAL INSTITUTE

SCIENTIFIC REPORT

00-09

Effects from high-speed civil traffic aircraft emissions on polar stratospheric clouds

By

Niels Larsen
Bjørn M. Knudsen
Michael Gauss
Giovanni Pitari

DMI

COPENHAGEN 2000

Effects from high-speed civil traffic aircraft emissions on polar stratospheric clouds.

Authors: Niels Larsen, Bjørn M. Knudsen, Michael Gauss, and Giovanni Pitari

Scientific Report 00-09

ISBN: 87-7478-416-1
ISSN: 0905-3263
ISSN: 1399-1949 (online)

Danish Meteorological Institute,
Ministry of Transport
Lyngbyvej 100,
DK-2100 Copenhagen Ø,
Denmark

Phone: +45 39 15 75 00
Fax: +45 39 27 10 80
www.dmi.dk

Effects from high-speed civil traffic aircraft emissions on polar stratospheric clouds.

Niels Larsen and Bjørn Knudsen
Danish Meteorological Institute, Denmark

Michael Gauss
University of Oslo, Norway

Giovanni Pitari
University of l'Aquila, Italy

This report constitutes the DMI-contribution to the final report of the EU project "Modelling of the impact on ozone and other chemical compounds in the atmosphere from airplane emissions" (AEROCHEM II, contract ENV4-CT97-0621, 1998-2000), funded by the European Commission Environment and Climate programme (4th Framework programme).

1. Introduction.

Emissions from stratospheric high-speed civil traffic (HSCT) aircraft may influence the probability of formation and the properties of polar stratospheric clouds (PSC). PSC particles play a decisive role for chemical ozone depletion in polar regions. The influence of PSC particles is two-fold. First, on the surfaces of the cloud particles, heterogeneous chemical reactions convert reservoir halogen compounds into potentially ozone destroying radicals, secondly the cloud particles may irreversibly remove reactive nitrogen (and water vapour) by gravitational sedimentation which may prolong the ozone depletion [*WMO*, 1999].

The cloud particles are composed of nitric acid and water, and stratospheric sulphate aerosols are believed to constitute the background particles, which serve as sites for PSC particle growth at low temperatures. New sulphate aerosol particles could be produced as a result of aircraft plume processing of SO_2/SO_3 and enhanced concentrations of SO_2, eventually oxidising into H_2SO_4, may in general increase the stratospheric sulphate mass mixing ratios and background aerosol concentrations. More directly may aircraft emissions of water vapour and NO_x, converting into HNO_3, lead to higher threshold temperatures for PSC formation and enhanced PSC particle surface area densities.

Only a few studies, applying more detailed PSC-microphysical schemes, have been performed to study the effects of stratospheric aircraft emissions on PSC properties [*Peter et al.*, 1991; *Pitari et al.*, 1993; *Considine et al.*, 2000]. A thorough review of the effects on PSC surface area densities, applying a selection of state-of-the-art atmospheric models with varying degrees of microphysical complexity, has been provided by *IPCC* [1999, cp. 4]. Common to most studies is the assumption of the existence of two types of solid phase PSC particles, forming at certain threshold temperatures (e.g. the nitric acid trihydrate (NAT) condensation temperature and the ice frost point). Subsequent research has revealed the existence of at least three PSC particle types, showing complicated transition processes between liquid and solid type particles which depend on the temperature histories of individual particles [e.g. *Larsen*, 2000a]. In this study a different approach has been taken, applying domain filling trajectories of a given Arctic winter, coupled with a detailed microphysical model, to investigate the effects of aircraft-enhanced concentrations of nitric acid and water vapour on PSC formation. The aircraft induced perturbations to HNO_3 and H_2O have been calculated by two 3D chemical transport models (3D-CTM), applying emissions scenarios provided by NASA. Although the threshold temperatures for the existence of different types PSC particles are marginally changed by increased concentrations of H_2O and HNO_3, the detailed microphysical simulations as presented below reveal a substantial enhancement of solid type PSC formation and the potential for stronger denitrification and dehydration.

2. PSC microphysics.

Two types of polar stratospheric clouds have been observed above the ice frost point: liquid particles (type 1b PSC), composed of supercooled ternary solutions (STS; $H_2SO_4/HNO_3/H_2O$), and solid particles (type 1a PSC), presumably composed of nitric acid trihydrate which is the stable nitric acid hydrate at stratospheric conditions. Furthermore, larger type 2 ice PSC particles form below the ice frost point temperature. The heterogeneous chemical reactions taking place on the surfaces of the PSC particles, activating halogen species, depend on the chemical compositions and physical phase of the particles. In addition, only solid type PSC particles are

responsible for denitrification and dehydration, i.e. the irreversible removal of reactive nitrogen and water by gravitational sedimentation of nitric acid holding particles.

The microphysical model from the Danish Meteorological Institute [*Larsen,* 2000b] comprehends all these PSC particle types. The model calculates the time dependent polar stratospheric cloud particle size distributions and chemical compositions together with changes in gas phase mixing ratios of water vapour and nitric acid vapour, assuming an initial size distribution of background sulphate aerosols and initial concentrations of H_2O and HNO_3. The model simulates the formation, growth, evaporation, and sedimentation of type 1b PSC particles (supercooled ternary solution, STS), type 1a PSC particles (assumed to be composed of nitric acid trihydrate, NAT), type 2 PSC ice particles, and frozen sulphate aerosol particles, assumed to be composed of sulphuric acid tetrahydrate (SAT). The model applies the basic vapour diffusion equation to calculate the exchange of mass between the gas and condensed phase during particle growth and evaporation. The model comprehends a number of possible pathways for phase changes and the formation of solid type PSC particles. This includes the calculation of homogeneous freezing rates of ice in STS particles to form solid type 2 PSC particles a few K below the ice frost point. The model also allows for heterogeneous nucleation of pre-activated SAT for the formation of type 1a PSC NAT particles in addition to deliquescence of SAT particles during cooling below the STS threshold temperatures and SAT melting at higher stratospheric temperatures. The model is written as an atmospheric box model, facilitating a coupling to chemical transport models and photochemical trajectory models.

One major obstacle to prescribing PSC formation in larger atmospheric chemistry models is the inherent temperature hysteresis in the particles' life cycle, changing between the liquid and solid phases. At decreasing temperatures the background sulphate aerosol particles take up nitric acid and water vapour, continuously turning into fully developed type 1b PSC particles at roughly 3-4 K below the existence temperature of NAT (T_{NAT}, roughly 195 K). The growth and changing in composition of type 1b PSC particles is illustrated in Figure 1. These particles survive in the liquid state, even to temperatures a few degrees below the ice frost point (8-10 K below T_{NAT}). The particles eventually freeze into type 2 PSC ice particles. During subsequent heating a residual of type 1a PSC particles can exist in the solid state at all temperatures below T_{NAT} before the remnant, possibly a solid sulphuric acid particle, melts at 210-220 K after all nitric acid in the particle has evaporated above T_{NAT}. Pathways may also exist for dissolution of solid sulphate aerosols, turning into type 1b PSC at low temperatures. NAT may also nucleate on pre-activated SAT particles at decreasing temperatures. Thereby the occurrence of a specific PSC particle type will depend on the actual temperature history and can only be modelled more accurately by a microphysical model when individual air parcel trajectories are known.

Figure 1 also illustrates the sensitivity of calculated type 1b PSC particle volumes and threshold temperatures to changes in nitric acid and water vapour gas phase concentrations. In these calculations the H_2O and HNO_3 gas phase concentrations have been changed by 20%. In particular the water vapour concentrations determine the ice frost point temperature and the homogeneous freezing rates of ice in STS. Increasing water vapour concentrations (e.g. caused by aircraft emissions) will imply higher freezing temperatures and more frequent solid type PSC formation and thereby the potential for enhanced denitrification. In focus of this project has been a study of expected changes in PSC properties due to changes in concentrations of H_2O and HNO_3 induced by stratospheric supersonic air traffic.

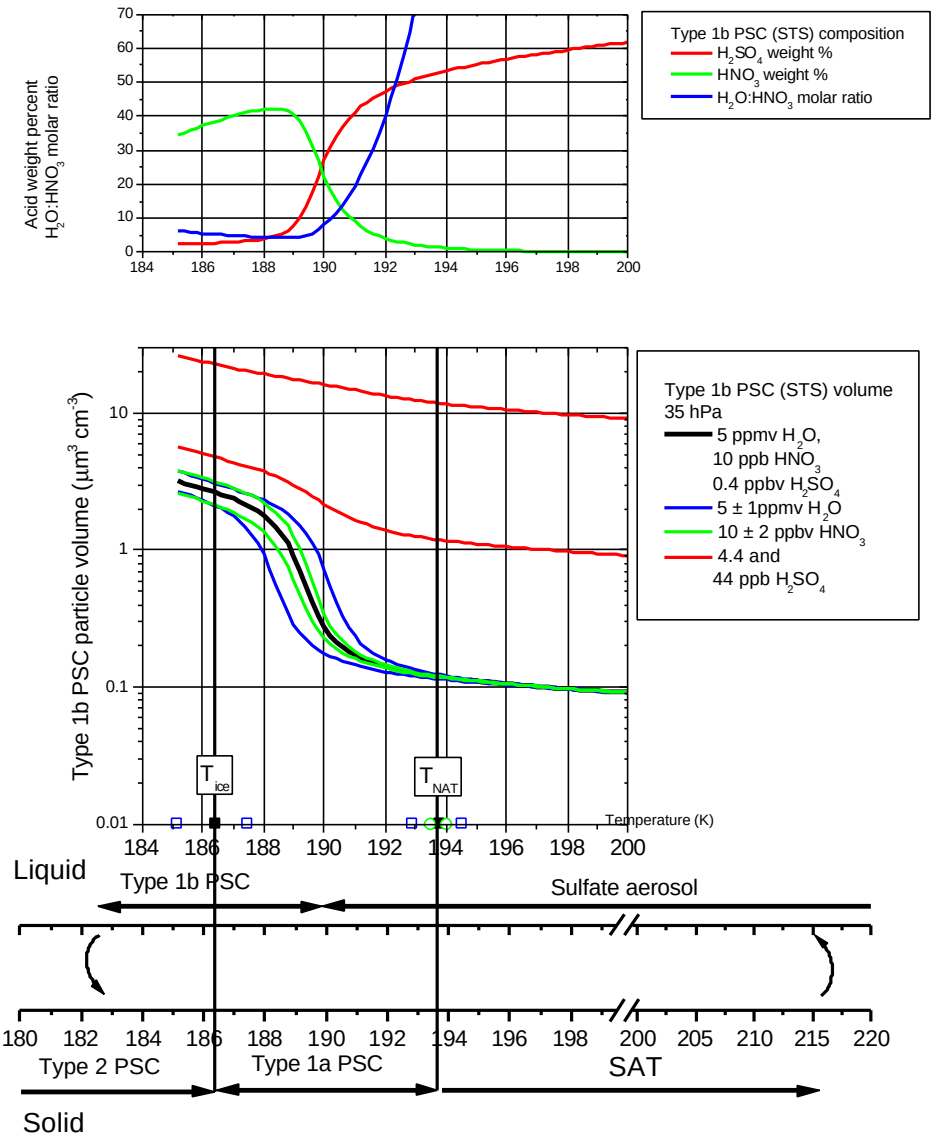

Figure 1. Type 1b PSC (STS) particle equilibrium chemical composition (upper panel) and volume (lower panel), calculated as function of temperature [*Carslaw et al.*, 1995] at 35 hPa, assuming 5 ppmv H_2O, 10 ppbv HNO_3, and 0.4 ppbv H_2SO_4 (black curve). The upper panel shows how the chemical composition continuously changes from a nearly binary H_2SO_4 solution through a ternary composition into a nearly binary HNO_3 solution at decreasing temperatures. In the lower panel, the blue curves indicate the volume range assuming 5±1 ppmv H_2O and the green curves assuming 10±2 ppbv HNO_3. The two red curves indicate the particle volumes, assuming 10 and 100 times increase in H_2SO_4, typical for volcanic conditions. T_{NAT} and T_{ice} are indicated on the temperature axis with the H_2O-variation range (blue square symbols) and the HNO_3-variation range (green circle symbols). The temperature axes in the lower part indicate the temperature existence range of different stratospheric particle types, showing the temperature hysteresis with freezing of liquid particles 3-4 K below T_{ice} and melting around 216 K.

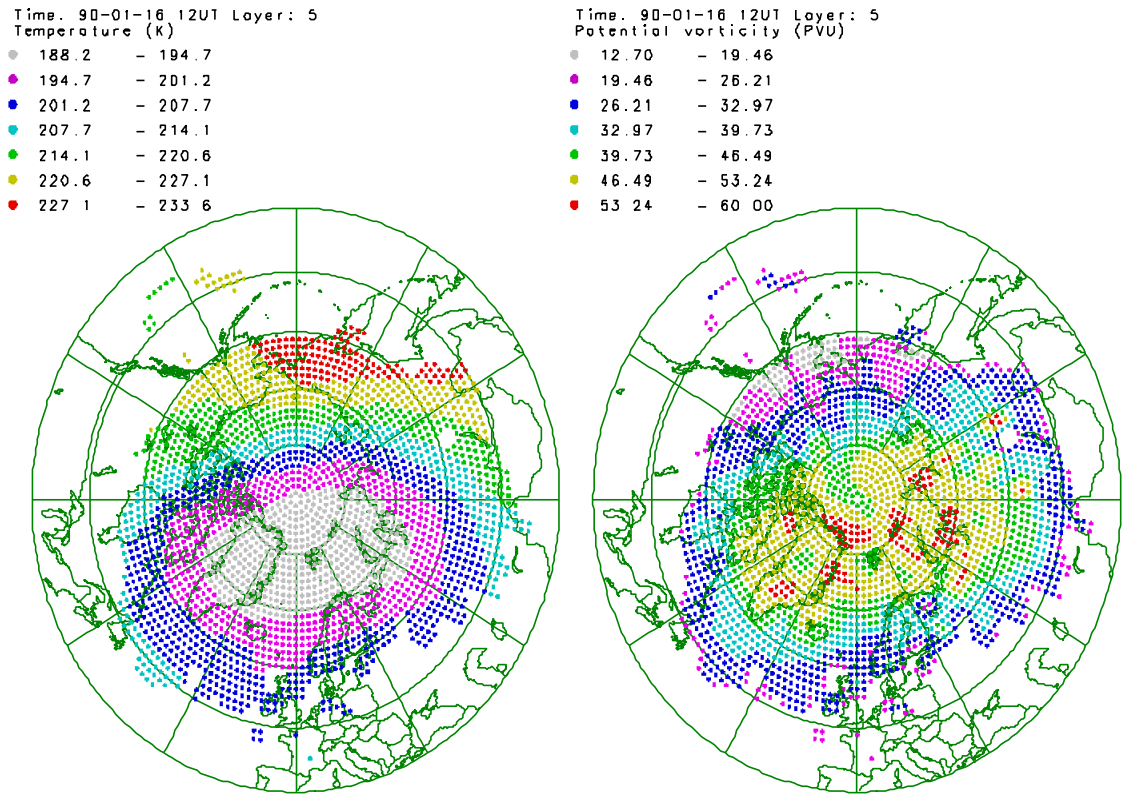

Figure 2 Plot showing the initial position of 2438 trajectory points on model level 5 at the potential temperature surface 475 K on 16 January 1990 at 12.00 UT. From this time in mid-winter, the trajectories are calculated backward in time until 1 December 1989 and forward in time until 1 March 1990 with a time resolution of 2 hours. The same holds for the other 8 model levels, giving a total of 23300 trajectories. The vortex edge is defined at 36 PV units at this potential temperature and at an equivalent modified PV value at other levels. (1 PVU = 10^{-6} K $m^2 s^{-1} kg^{-1}$).

3. Domain filling trajectories.

Many previous studies [*IPCC*, 1999] have calculated PSC properties in fixed grid points in larger atmospheric circulation models. In this investigation, calculations of the occurrence and surface area densities of PSCs are performed in a Lagrangian way, based on coupled domain filling trajectories and detailed microphysical simulations and using analysed temperatures from a representative winter (1989/1990) in the northern hemisphere. Thereby the temperature histories of individual PSC particles are used as input to calculate PSC properties. The winter 1989/1990 was relatively cold from mid December to mid February when the area with temperatures below T_{NAT} at 30 hPa covered between 2 and 4% of the NH (25-50 % of the area north of 67°N) [*Pawson et al.*, 1995; *Manney et al., 1994*]. The same representative temperatures from this winter have been used in different scenarios, assuming aircraft induced perturbations to the gas phase concentrations of H_2O and HNO_3.

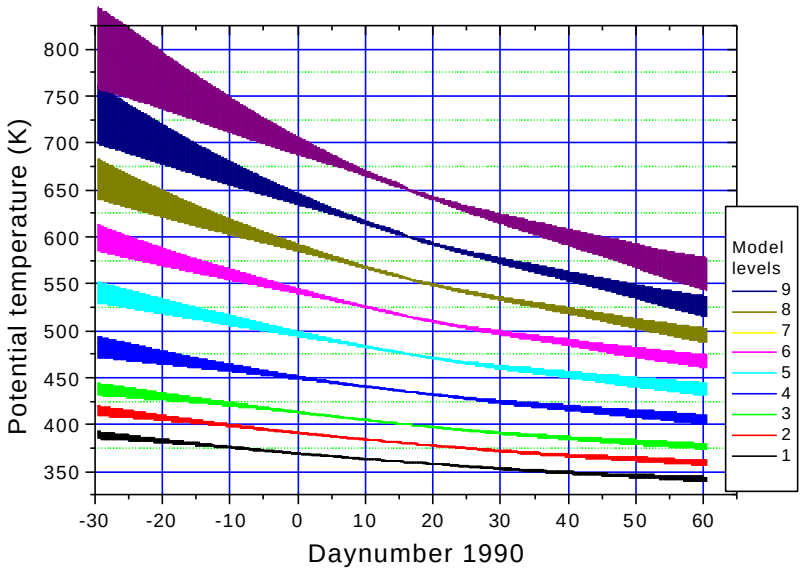

Figure 3 Average potential temperature and standard deviations (width of the curves) for trajectories on the nine model levels as function of time throughout the winter 1989/1990.

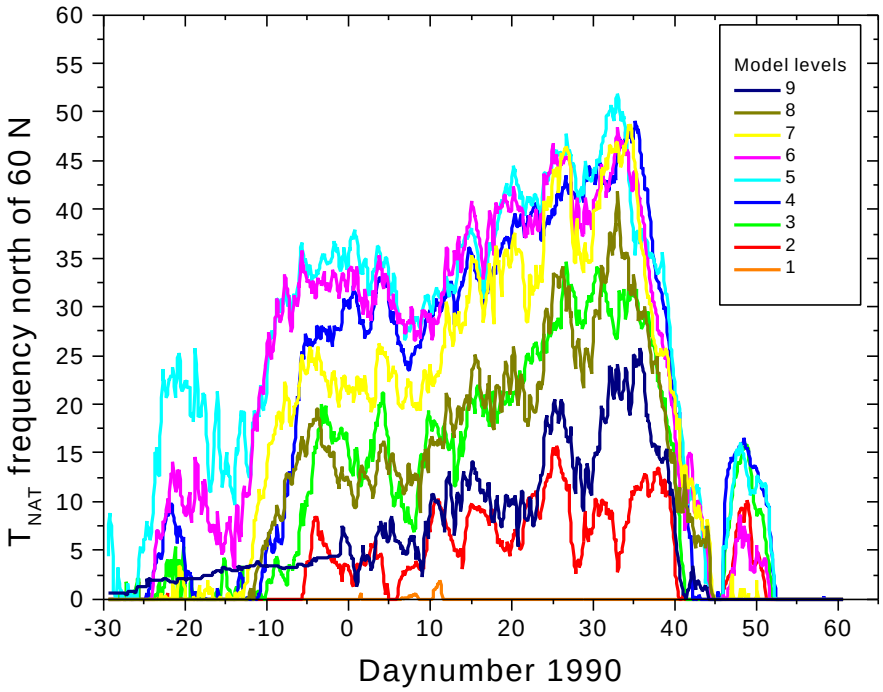

Figure 4 Fraction of locations on the nine model levels inside the northern hemisphere polar vortex with temperatures below T_{NAT} (assuming no aircraft emissions).

The domain-filling trajectory calculations use 6 hourly ECMWF (European Centre for Medium-Range Weather Forecasts) analyses in a 1.5 degree latitude-longitude grid. They are performed in an equal-area grid with a grid-distance of 139 km (1.25° of latitude) and start at 9 isentropic levels inside or at the edge of the polar vortex and north of 60°N. The trajectory data are stored for every 2 hours. The trajectories are calculated both backward and forward in time for 45 days from 16 January 1990 covering the whole PSC season in this winter from the beginning of December 1989 to the end of February 1990. The results are 23300 trajectories of 90-day duration, which are necessary for the PSC box model, but which become increasingly inaccurate away from 16 January 1990. The bulk advection is, however, reasonably well represented in such extended calculations [e.g. *Manney et al*., 1995; *Morris et al.*, 1995; *Knudsen and Grooß*, 2000]. The potential temperature in each time step is decreased by the diabatic heating in each time step. The clear-sky heating rates are calculated with the ECMWF radiation scheme [*Morcrette*, 1991] and they are described in *Knudsen and Grooß* [2000].

The location of the initial points on model level 5 at 475 K potential temperature is illustrated in Figure 2 showing the temperature and potential vorticity. Since most of the trajectory points are initialised inside the polar vortex there is relatively little geographical spread in the trajectories going backward and forward in time from the mid-winter initial time. In the following calculations the vortex edge has been set at a potential vorticity of 36 PV units at potential temperature θ=475 K and at the equivalent value of modified potential vorticity [$MPV=PV\cdot(475K/\theta)^{4.5}$] at the other potential temperature surfaces. Radiative cooling leads to an average decrease in potential temperature throughout the winter. Figure 3 illustrates the average potential temperature and standard deviation for all trajectories on the 9 model levels.

In Figure 4 is shown the fraction of locations on the nine model levels inside the polar vortex with temperatures below T_{NAT}. Temperatures reach the lowest values with most PSC formation on levels 4, 5, and 6 and calculation on these levels will be in focus in the following analysis.

The temperature histories from the trajectories have been used as input to the microphysical model to calculate PSC particle surface areas, chemical compositions, physical phase of the particles, and gas phase concentrations of HNO_3 and H_2O at each trajectory point throughout the winter.

The microphysical model has been initialised with aerosol surface areas, consistent with a SAGE I and II surface area climatology [*Hitchman et al.*, 1994]. Figure 5 shows

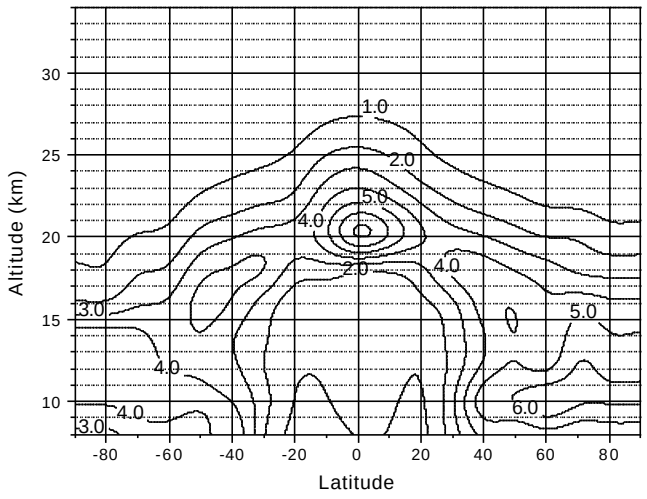

Figure 5. Applied sulphate aerosol surface area densities, consistent with SAGE extinction measurements [*Hitchman et al*., 1994]

the applied surface area densities. Number densities of sulphate aerosols (N) are derived from the surface area densities (A), assuming that the particles are characterised by a lognormal size distribution with median radius r_m=0.0725 μm and a geometric standard deviation σ=1.86, i.e. $A = N\,4p\,r_m^{\,2}\exp\left[2(\ln s)^2\right]$. Initial concentrations of nitric acid and water vapour are provided by the 3-D CTM at University of Oslo and the University of l'Aquila, applying different aircraft emission scenarios.

Figure 6 illustrates an example of calculated fields of type 1a and type 1b PSC surface area density and gas phase concentrations of HNO_3, based on background ("no-aircraft") HNO_3 and H_2O conditions from the Oslo CTM model.

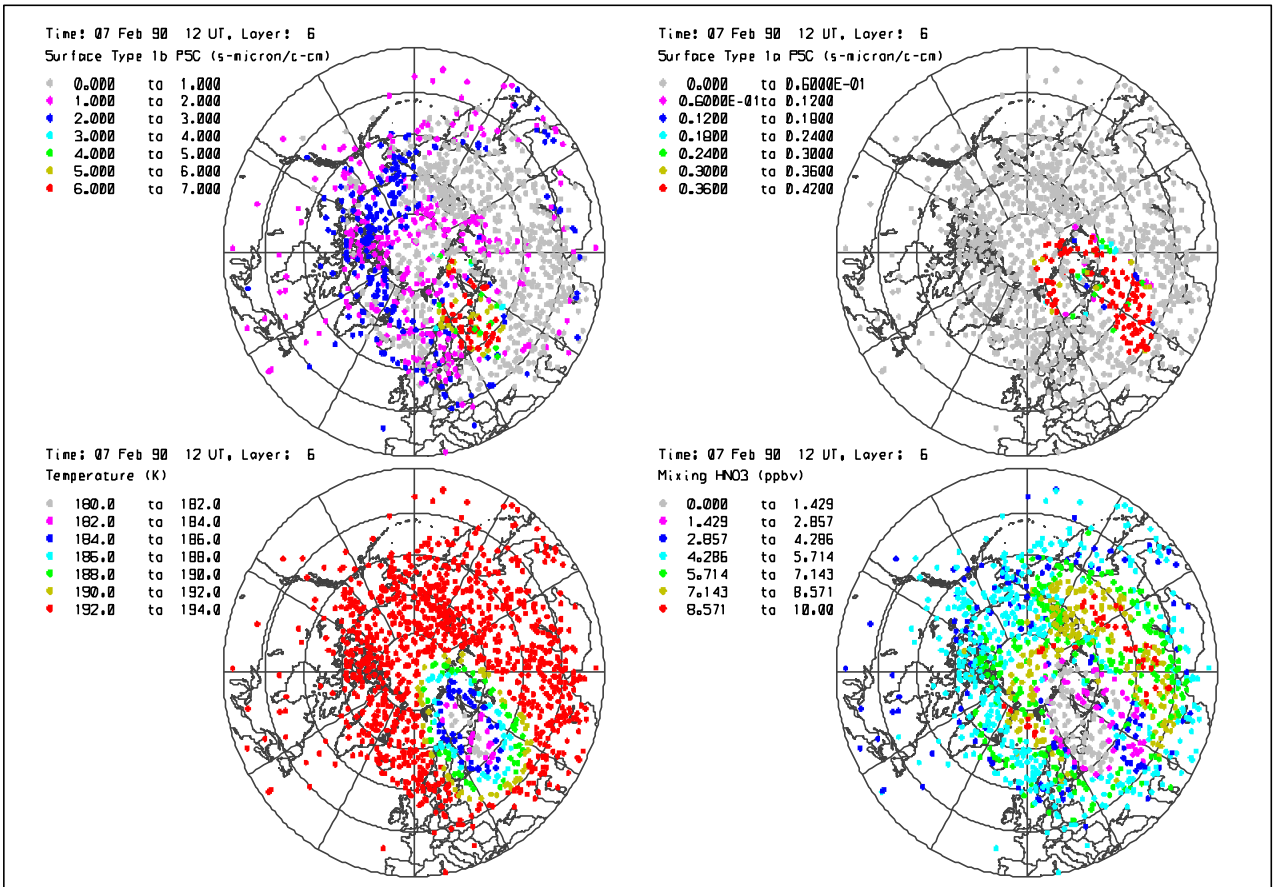

Figure 6 Calculated surface area densities of type 1b PSC (upper left panel) and type 1a PSC (upper right) together with gas phase HNO_3 (lower right) on 7 February 1990, 12.00 UT at model level 6. The lower left panel shows the temperature field.

4. Chemical transport models.

Both the stratospheric chemical transport models at the University of Oslo (UiO) and at the University of l'Aquila (ULAQ) have been used to provide perturbed fields in HNO_3 and H_2O due to aircraft emissions of nitrogen oxides and water vapour.

The SCTM-1 at UiO is a global 3-dimensional stratospheric chemical transport model. The resolution is 7.8° latitude x 10° longitude in 29 layers extending from the surface up to 90 km. The vertical layers are defined in sigma coordinates below 100 hPa and in pressure coordinates above. The transport is driven by wind fields from the GISS GCM [*Rind et al*., 1988], while temperatures are from daily National Center for Environmental Prediction (NCEP) global analyses for 1990.

The chemistry code [*Stordal et al*., 1985, *Isaksen et al*., 1990] includes 55 species and focuses on stratospheric chemistry. 104 thermal and 47 photolytic reactions are integrated by the QSSA method [*Hesstvedt et al*., 1978]. Although the chemistry module has not been designed for detailed tropospheric or mesospheric studies, ozone production from methane is included so that the code is basically applicable in the upper troposphere as well. Seven heterogeneous reactions are simulated on stratospheric sulphate aerosols and/or on type 1 PSCs including heterogeneous processing of reactive chlorine, bromine, and nitrogen. The photolysis rate calculation is done on-line by the module of *Kylling et al*. [1995], recalculating and archiving the diurnal cycles for the 3-D model grid every 7 days. The ozone distribution, air density, and temperatures used in this calculation are taken directly from the model during runtime. As the time step for chemistry integrations is 10 minutes and the photolysis rates are resolved at intervals of 40 min, the chemical solution is iterative.

The advection scheme applies the concept of Second Order Moments [*Prather*, 1986], which is an upstream scheme taking into account the sub-grid scale distribution of mass and transported tracers. The use of the moments leads to an effective resolution that is 3 times the formal grid resolution. Tropospheric convection and horizontal diffusion in SCTM follow *Prather et al*. [1987,1990]. In moist convection, 50% of the mass is taken from the originating layer and put to the receiving layer, while dry convecton causes complete mixing. While the transport algorithms cover the whole model domain, chemistry integrations are done only between about 6 and 55 km. Boundary conditions at the surface and the model top are derived from multi-year runs of the OSLO 2D model [*Isaksen et al*., 1990]. Mesospheric initialization of SCTM is done by calculating scale heights at 50 km, which are used to extrapolate the fields from the Oslo 2D model upward. For a detailed description of the original 21-layer version see *Rummukainen* [1996] and *Rummukainen et. al.* [1999]. It must be noted that in this study a higher resolution was implemented in the upper troposphere and the lower stratosphere, taking advantage of the SOM transport scheme, whereby the number of model layers increased to 29.

As a model year, 2015 was chosen to illustrate future aircraft impact. The background atmosphere is based on the IPCC emission scenario IS92a [*IPCC*, 1995]. The scenarios for aircraft emissions are from the NASA data base [*Baughcum et. al*, 1998]. Emissions of NO_x and water vapour from sub- and supersonic aircraft were considered. Three different cases were calculated: 1) 'No aircraft' emissions, 2) subsonic emissions only, and 3) both sub- and supersonic emissions (designated 'supersonic' scenario in the following). Each case was integrated for 7 years with constant emissions in order to get stable results for the perturbations.

For the supersonic aircraft emissions a fleet consisting of 500 aircraft with an emission index E.I.(NOx)=5 was chosen (5 grams of NO_x are emitted for each kg of burnt fuel). For H_2O emissions the assumption was E.I.(H_2O)=1230. The perturbations were calculated in a 3-dimensional grid for 01 December 2015 for each of the three cases. Modelled HNO_3 is increased by up to 25 % at mid northern latitudes due to the inclusion of subsonic aircraft.

Supersonic aircraft lead to a secondary maximum increase of 12% in the lower tropical stratosphere. Subsonic aircraft do not perturb water vapour concentrations significantly, while an increase of up to 14% due to supersonic aircraft is modelled at mid northern latitudes at about 18 km altitude.

Figure 7 illustrates background ('no aircraft') concentrations of H_2O and HNO_3 and the calculated perturbations in H_2O and HNO_3 for the 'supersonic' scenario in the UiO model.

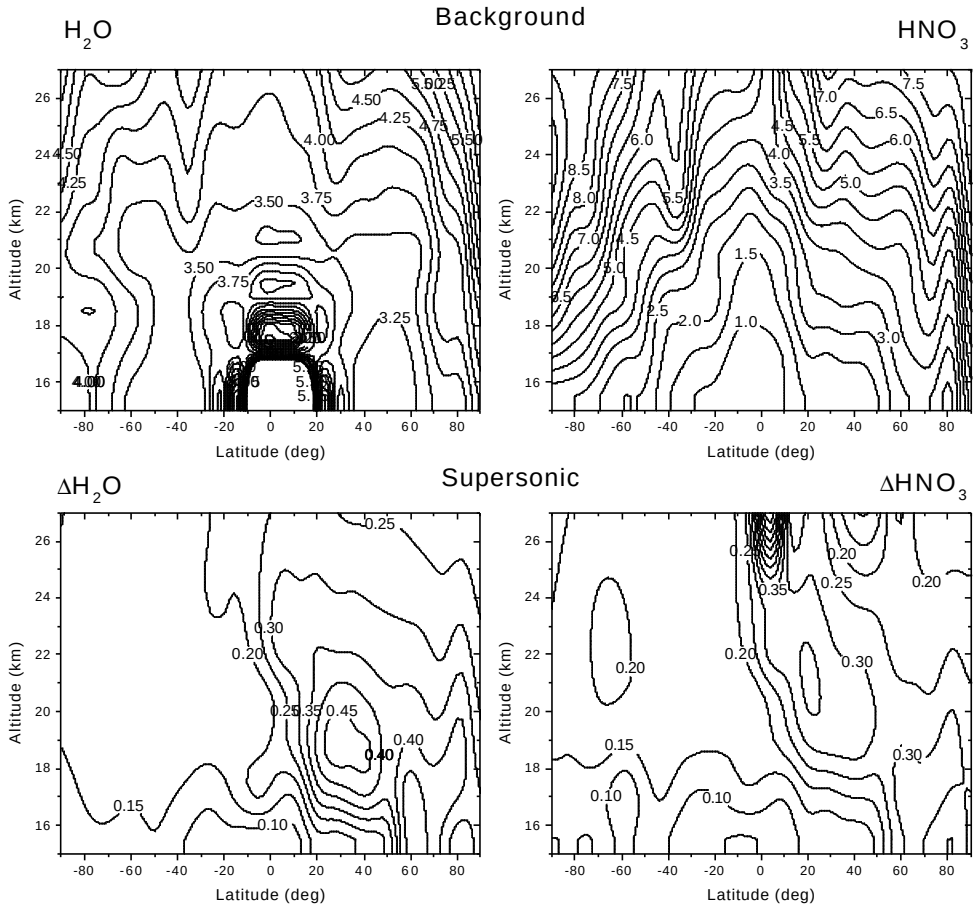

Figure 7 Applied background ('no aircraft') concentrations of water vapour (upper left panel, ppmv) and nitric acid (upper right, ppbv), and perturbations to these concentrations in the 'supersonic' scenario (shown in the panels below), using data from the University of Oslo model.

As a rough estimate, the ice frost point temperature will increase by a little more that 1 K for an increase in water vapour of 1 ppmv, meaning that the H_2O perturbations shown in Figure 7 will imply an increase in frost point temperatures on the order of 0.2-0.4 K. An increase of HNO_3 by 1 ppbv only causes an increase in the condensation temperature of NAT (T_{NAT}) of a few tenths of a degree whereas T_{NAT}, like the frost point temperature, increases by roughly 1K for an increase of 1 ppmv H_2O. Therefore the perturbations in H_2O will have the strongest influence on the aircraft induced perturbations.

In the University of l'Aquila model, all calculations were made with a low-resolution 3D-CTM. The basic features of the model are as follows. The grid is made by 26 log-pressure levels extending from the surface up to about 71 km altitude, while horizontally there is a 10x20 degrees resolution in latitude-longitude. The chemical code includes stratospheric families and the most important hydrocarbons for a realistic tropospheric chemistry parameterisation. Transport includes advection, vertical diffusion, weak horizontal diffusion and deep convection. A microphysical code for SSA, PSC (NAT and ice), and tropospheric aerosols (carbonaceous, dust, seasalt) is on-line with the model in a gas-particle mass conserving framework.

Subsonic and future supersonic aircraft are included using the NASA emission scenarios released in 1996 and appropriate for the year 2015 (data available on the Langley UADP database). The corresponding version of the 2D model has used the same emission data for the *IPCC* [1999] assessment. HSCT emissions considered here are those of NO_x, H_2O, SO_2, black carbon soot, CO, CO_2 and hydrocarbons (as CH_4). Additional formation of sulphate particles is obtained in two ways: enhanced condensation of gas phase H_2SO_4 (formed through SO_2 oxidation) and direct particle production in aircraft plumes, assuming a 10% conversion fraction of the emitted SO_2. Emission indices used here and those realistically predicted for the year 2015 technology, that is (in g/kg-fuel): 1237 (H_2O), 5 (NO_x), 0.4 (SO_2), 0.04 (soot), 1.0 (CO), 3155 (CO_2), 0.2 (CH_4).

H_2O emissions may also perturb the radiation budget in the lower stratosphere, with a potential feedback on species transport; this effect has not been deeply investigated so far. The ULAQ group has made some preliminary studies using a stratospheric GCM.

Water vapour heats the lower stratosphere by absorbing black body radiation from the troposphere and near infrared radiation from the sun, and cools the stratosphere by emitting longwave radiation to space. The combination of heating and cooling produces net heating rates that are positive in the lower stratosphere tropical region and negative at mid-high latitudes, mainly in the winter hemisphere. This is because the tropical lower stratosphere is colder (less cooling to space), the underlying troposphere is warmer (more heating form below), and because there is less incoming solar radiation in the winter mid-high latitudes.

The contribution of H_2O to the stratospheric diabatic circulation will add to those of O_3 and CO_2: the Brewer-Dobson circulation shows on average tropical upwelling and wintertime extratropical subsidence. With an increase of stratospheric H_2O, like that produced by supersonic aircraft, we may expect an enhancement of the diabatic circulation, with a resulting perturbation of the stratosphere-troposphere ozone flux as well as changes in the large-scale distribution of other chemical tracers in the lower stratosphere (NO_y, Cl_y, H_2O itself). Concentrations of H_2O and HNO_3, calculated by the ULAQ model and including the H_2O radiative feedback, will be designated the 'supersonic-radiative' scenario in the following. Figure 8 shows the background concentrations of H_2O and HNO_3, and the perturbations in the 'supersonic' and 'supersonic-radiative' scenarios.

Calculations have been performed with the microphysical model, using the same trajectories and temperature histories as for the 1989/1990 winter, but assuming perturbed fields nitric acid and water vapour, based on the 2015 scenarios of NO_x and H_2O emissions from subsonic+supersonic aircraft, calculated by the CTMs at the University of Oslo and University of l'Aquila. Calculations have also been performed for the subsonic aircraft scenario, showing only a modest influence on the PSC properties. Therefore, only the 'supersonic' scenarios will be compared to the 'no aircraft' emission scenario in the following.

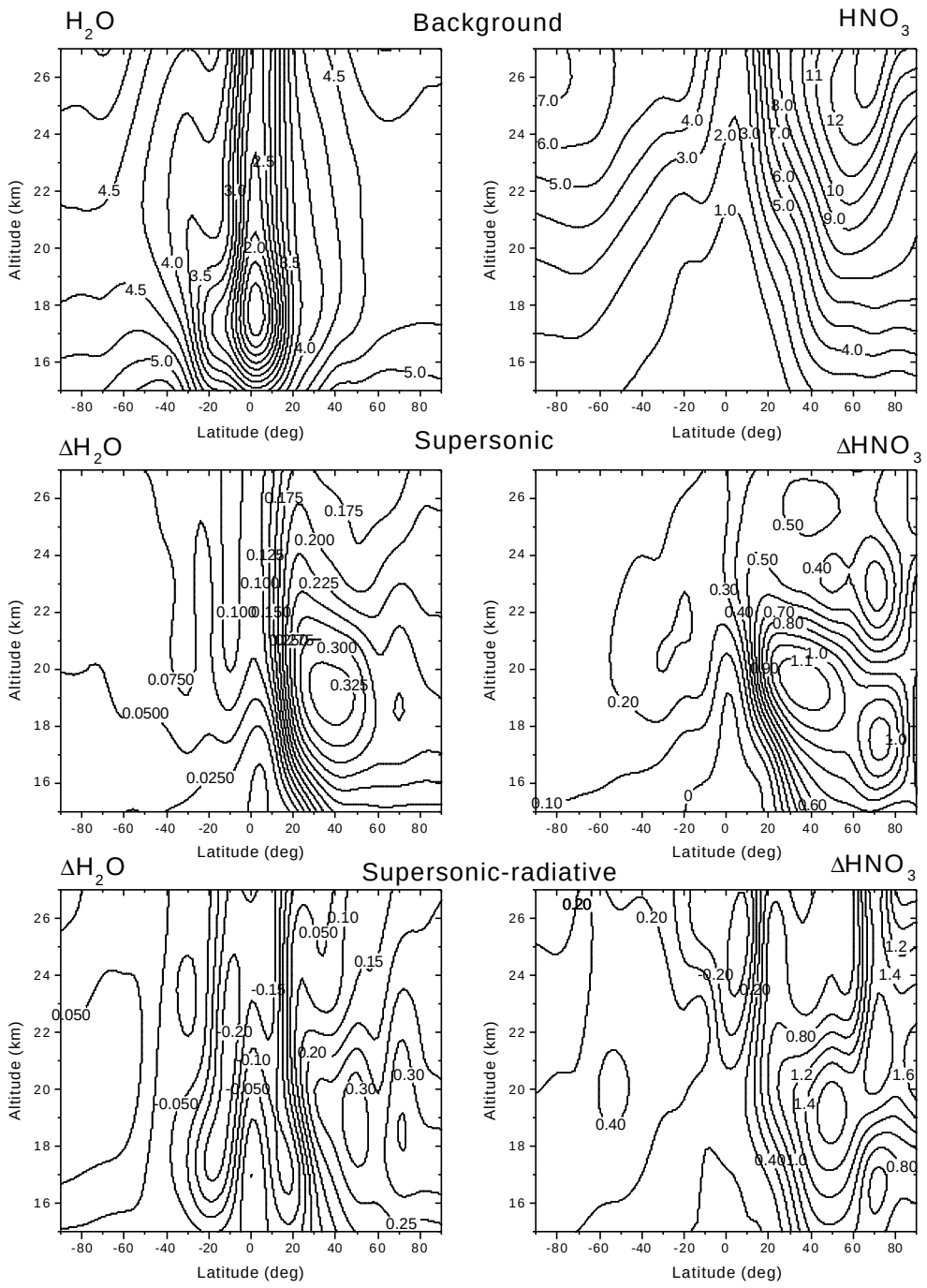

Figure 8 Background concentrations of H_2O (upper left, ppmv) and HNO_3 (upper right, ppbv) from the University of l'Aquila model together with 'supersonic' (middle row) and 'supersonic-radiative' (lower row) perturbations.

5. Calculated PSC properties.

Figure 9 shows changes in occurrence of locations inside the polar vortex with temperatures below T_{NAT} in model levels 4, 5, and 6. The upper curves in each panel show the results for the UiO 'no aircraft' scenario (similar to Figure 4) whereas the thin lower curves show the difference between 'supersonic' and 'no aircraft' conditions. The fraction of locations inside the polar vortex with temperatures below T_{NAT} typically increase 2-5% and up to 10% in model level 4 in early winter due to the changes in HNO_3 and H_2O.

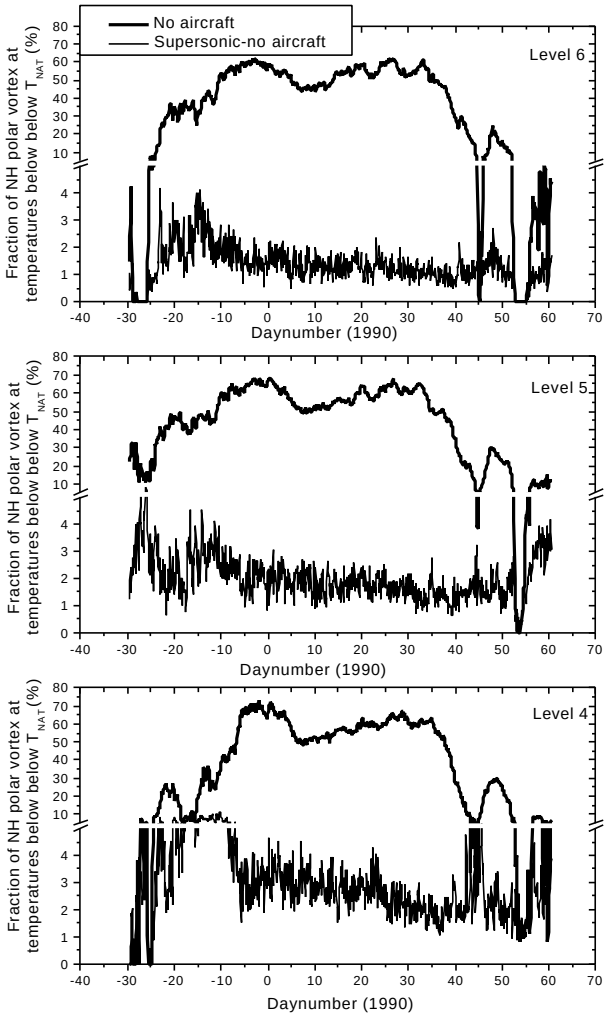

Figure 9. Fraction of locations inside the NH polar vortex with temperatures below T_{NAT} ('no aircraft', upper thick curve) and the difference between 'supersonic' and 'no air craft' conditions (lower thin), using the UiO model perturbations at model levels 4, 5, and 6. Note the difference in ordinate scale.

The type 1b PSC equilibrium model of *Carslaw et al.* [1995] has also been used to calculate the associated changes in vortex-averaged particle volumes (cf. Figure 1) due to changes is HNO_3 and H_2O concentrations, calculated by the UiO model as shown in Figure 10. The increased gas phase concentrations give rise to increases in type 1b PSC particle volumes of about 10% inside the polar vortex in the 'supersonic' conditions, compared to the 'no aircraft' scenario.

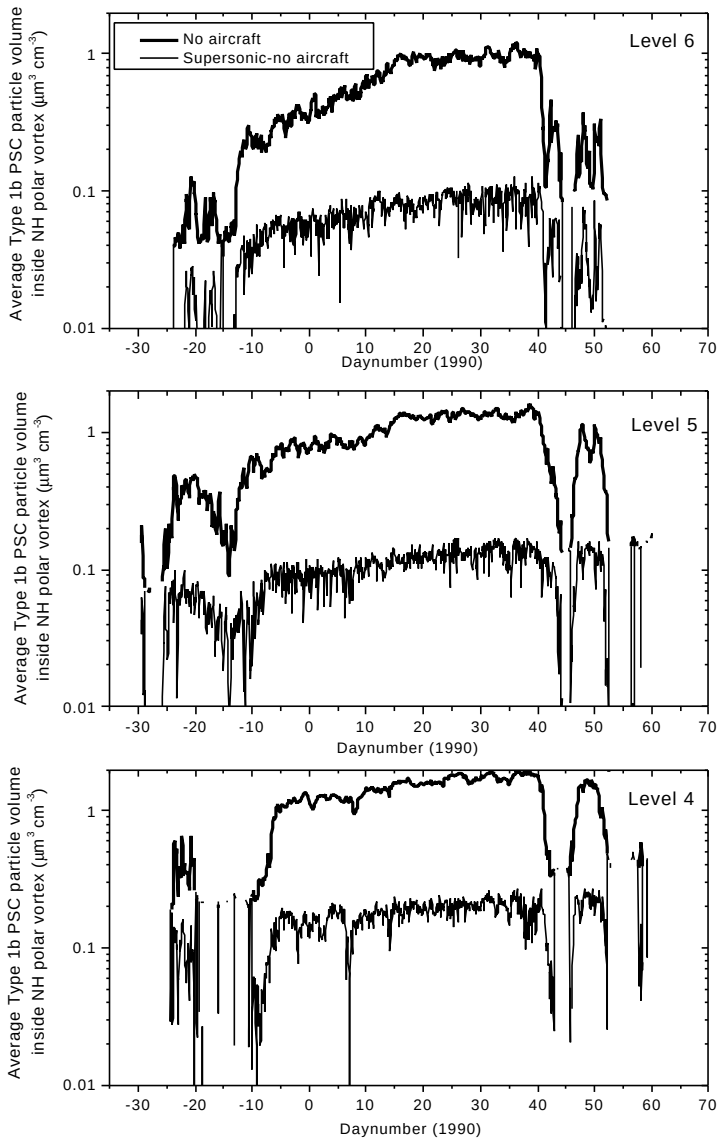

Figure 10. The STS type 1b PSC equilibrium model of *Carslaw et al.* [1995] has been used together with temperatures from the trajectory model to calculate average particles volumes inside the polar vortex at model levels 4, 5, and 6. The upper thick curve shows the vortex-averaged type 1b PSC particle volumes for the 'no aircraft' conditions (UiO model) and the lower thin curve the difference in calculated particle volumes between the 'supersonic' and ' no aircraft' scenarios.

The calculations of changes in occurrence of temperatures below T_{NAT} (Figure 9) and volumes of type 1b PSC particles (Figure 10) are only threshold conditions, based exclusively on vapour pressures of NAT and STS, respectively, without any microphysical assumptions about the actual PSC formation under the changing conditions. Therefore the temperature histories from the trajectories have been used as input to the microphysical model, performing simulations of the PSC formation under the two aircraft emission scenarios. Figure 11 shows the calculated frequency of occurrence of three different types of PSCs inside the polar vortex. The frequencies

are calculated as the percentages of trajectory points inside the polar vortex where the model shows that PSC particles of the different types exist. The gray shaded curves show the 'no aircraft' scenario and the thick curves the 'supersonic' scenario, using the University of Oslo model perturbations.

First it should be noticed from the 'no aircraft' results that the frequency of PSC occurrence is substantially smaller that the frequency when temperatures drop below T_{NAT} (cf. Figure 9), pointing out that assumptions about PSC formation below T_{NAT} could be a simplified assumption to be applied in atmospheric chemistry models, in particular in marginal cold winters.

As it would be expected the 'supersonic' scenario emission only give rise to an increase in type 1b PSC occurrence of a few percent since the formation of this type of clouds only depend on the STS threshold temperature conditions.

However, a much more pronounced difference between the two scenarios is seen in the occurrence of solid type 1a and type 2 PSCs. Solid type PSCs are assumed only to form when ice freezes out of STS solution 3-4 K below the ice frost point. The homogeneous freezing rate depends on the water vapour partial pressure (and temperature) and increased concentrations of H_2O lead to more widespread freezing and solid type PSC formation.

Figure 12 shows the vortex-averaged surface area densities of the different PSC types. A substantial increase in solid type PSC surface area is seen between the two emission scenarios. It should be noticed that in particular the increase in type 2 PSC ice particle surface areas may have implications for heterogeneous chemical activation.

It is also important to note that only solid type PSC particles may induce denitrification and dehydration. A potential exists that the enhanced H_2O concentrations, caused by stratospheric aircraft emissions, may lead to more solid type PSC formation and thereby more widespread denitrification.

In order to quantify this potential for enhanced denitrification, model runs have also been performed, using the University of Oslo model perturbations, where the gravitational sedimentation of particles is included. In principle it is not possible in a domain filling trajectory approach to make an accurate calculation of denitrification over a large span in altitude since the in-fall of particles from layers above (renitrification) cannot be exactly represented. However, the fall-out of particles from trajectories in a given layer can be calculated with high accuracy and thereby how much HNO_3 and H_2O is left in the gas phase after all remaining particles are evaporated. Results from a calculation of this kind are shown in Figure 13.

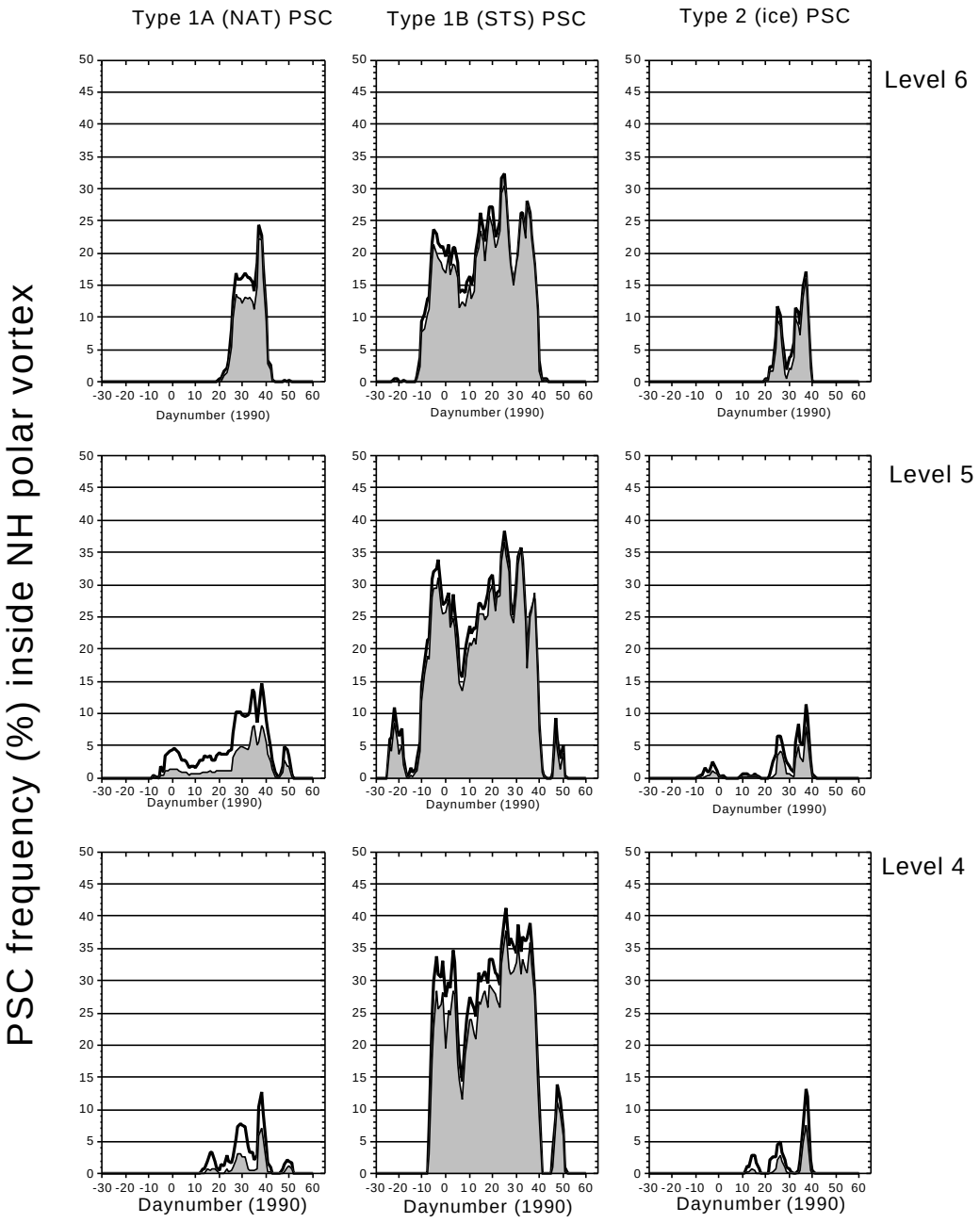

Figure 11 Frequency of the occurrence of type 1a PSCs (left column), type 1b PSCs (middle) and type 2 PSCs (right) at model levels 4, 5, and 6 in the 'no aircraft' emission scenario (gray shaded curves) and the 'supersonic' scenario (black curves), using the University of Oslo-model aircraft induced perturbations in H_2O and HNO_3 concentrations.

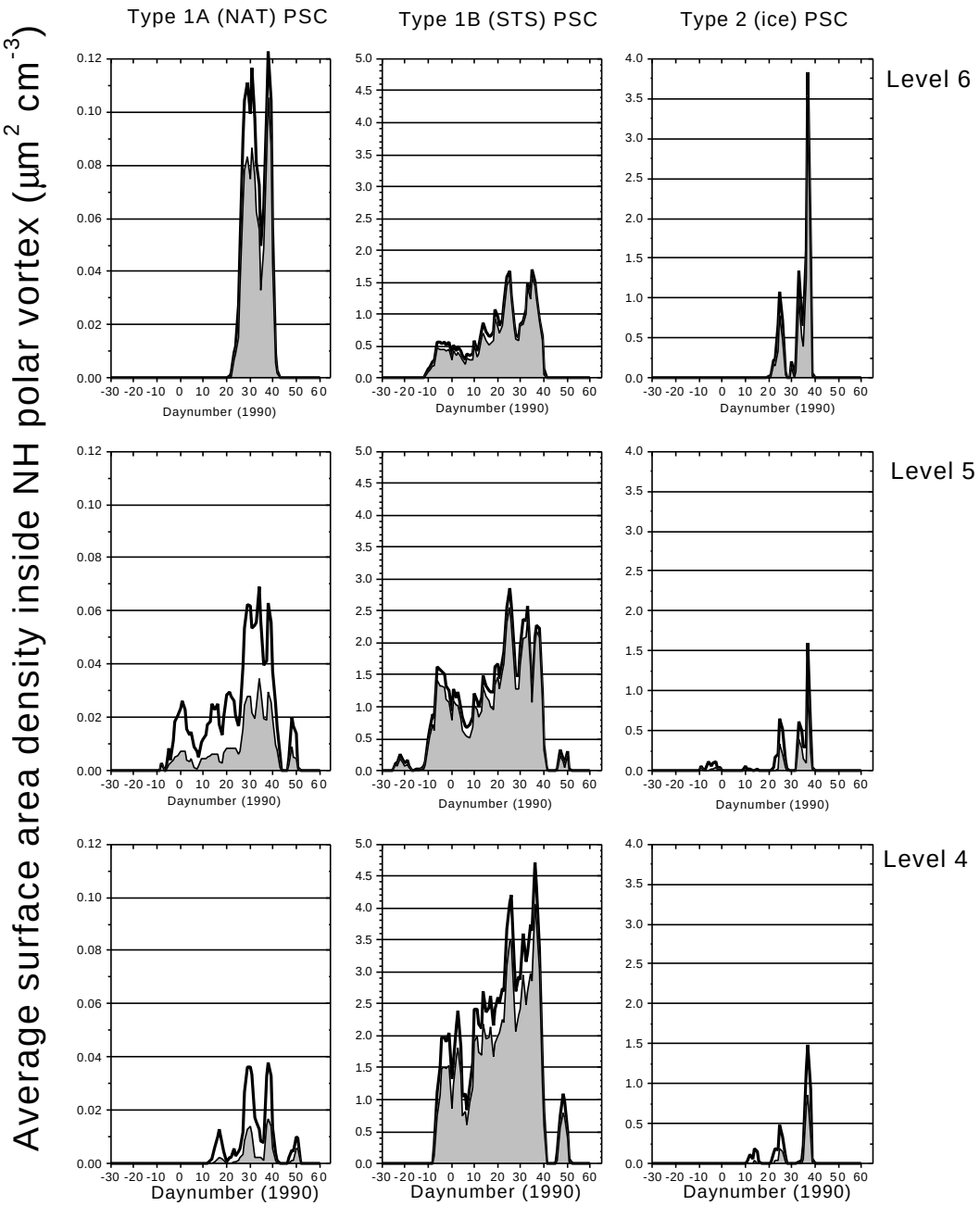

Figure 12 Vortex-averaged surface area densities of type 1a PSCs (left column), type 1b PSCs (middle) and type 2 PSCs (right) at model levels 4, 5, and 6 in the 'no aircraft' emission scenario (gray shaded curves) and the 'supersonic' scenario (thick curves), using the University of Oslo-model aircraft induced perturbations in H_2O and HNO_3 concentrations. Notice the difference in ordinate scales in the three columns

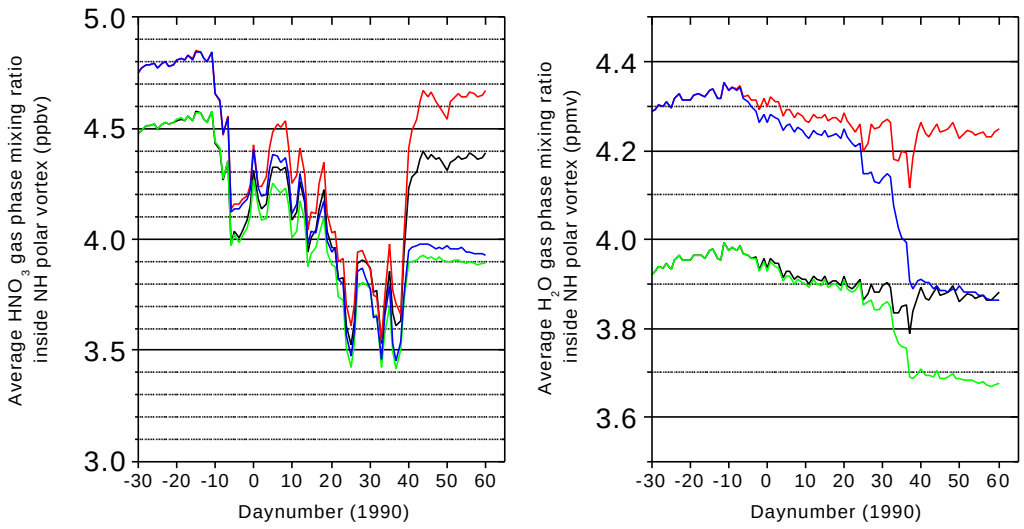

Figure 13 Comparison of simulated denitrification (left) and dehydration (right) due alone to gravitational particle fall-out of layer no. 5 (i.e. no compensation for in-fall of particles from layers above is included in the calculations). The black and red curves show the vortex-averaged gas phase concentrations with no sedimentation included in the 'no aircraft' and 'supersonic' cases, respectively, using the University of Oslo-model aircraft induced perturbations in H_2O and HNO_3. The difference between these two curves represents the difference in concentrations due to aircraft emissions. The green and blue curves show for the 'no aircraft' and the 'supersonic' cases, respectively, the mixing ratios with sedimentation of the particles included in the calculations. In this case the difference between the blue and green curves decreases with time, reflecting the enhanced denitrification and dehydration in the 'supersonic' case, compared to the 'no aircraft' scenario.

The difference between the black and red curves in Figure 13, representing the 'no aircraft' and 'supersonic' scenarios and not including particle sedimentation simply reflects the enhanced mixing ratios caused by the aircraft emissions. The temporary drops in mixing ratios reflect the uptake from the gas phase by condensation into the particles.

The results from the calculations including sedimentation show the difference in mixing ratios between the 'supersonic' and 'no aircraft' mixing ratios decreases throughout the winter, meaning that a larger denitrification and dehydration takes place in the 'supersonic' scenario. At model level 5, where the relative increase in occurrence of solid type PSC is largest, the HNO_3 mixing ratio decrease from 4.47 to 3.89 ppbv due to particle fall-out in the 'no aircraft' scenario (green curve in left-hand panel in Figure 13). The decrease is from 4.76 to 3.93 ppbv HNO_3 in the 'supersonic' scenario (blue curve). In the no-sedimentation cases there is a slight drop in HNO_3 mixing ratios of 0.08 ppbv (due to transport). Correcting for this means that there is a potential for stronger denitrification of about 38%. Likewise the 'no aircraft' scenario shows a drop in H_2O mixing ratio of about 0.24 ppmv from 3.92 to 3.68 ppmv (green curve in right-hand panel), compared to a drop of 0.43 ppmv from 4.29 to 3.86 ppmv in the 'supersonic' case, i.e. an increase in potential dehydration of 68% after correcting for the transport effects of 0.04 ppmv.

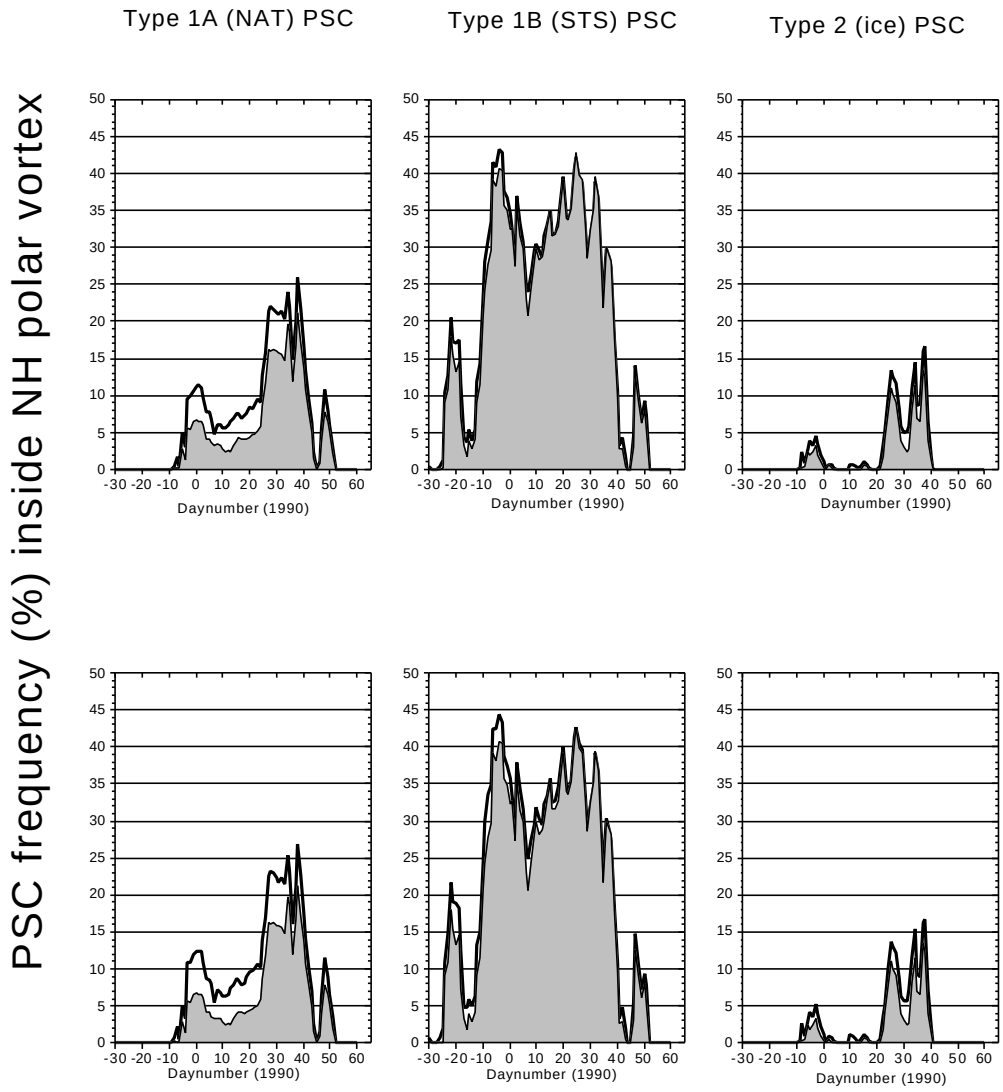

Figure 14 Frequency of occurrence of different types of PSC at model level 5, calculated using the University of l'Aquila model data for H_2O and HNO_3 concentrations and aircraft induced perturbations. The gray shaded curves in all panels show the 'no aircraft' scenario. The thick curves in the upper row show the 'supersonic' scenario, whereas the blue curves in the lower row show the results for the 'supersonic-radiative' scenario.

Calculations have also been performed for model level 5, using the H_2O and HNO_3 concentrations and aircraft induced perturbations from the University of l'Aquila model. Figure 14 shows the calculated frequency of occurrence of the three PSC particle types and Figure 15 the calculated vortex-averaged surface area densities.

First it can be noticed that the frequency of occurrence in the 'no aircraft' scenario, using the University of l'Auila data compared to the Oslo data, are larger due to higher HNO_3 concentrations (cf. Figure 11). Also the frequency of solid type PSC is higher due to higher H_2O concentrations (cf. Figures 7 and 8).

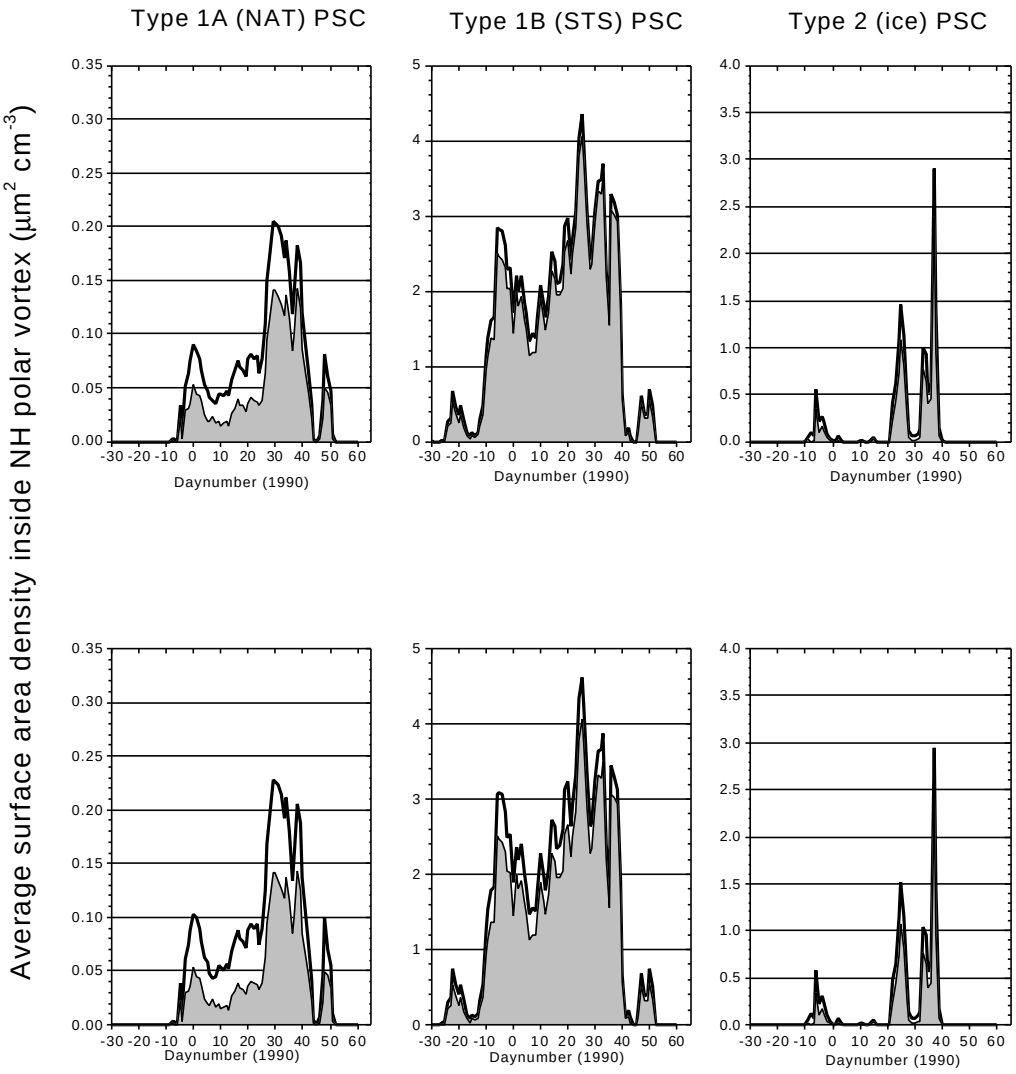

Figure 15 Vortex-averaged surface area densities of different types of PSC at model level 5, calculated using the University of l'Aquila model data for H_2O and HNO_3 concentrations and aircraft induced perturbations. The gray curves in all panels show the 'no aircraft' scenario. The black curves in the upper row show the 'supersonic' scenario, whereas the black curves in the lower row show the results for the 'supersonic-radiative' scenario.

Again, a pronounced difference in the occurrence and surface area densities for solid type PSC particles is calculated, caused by the "supersonic" aircraft emissions whereas the influence on liquid type 1b PSC is moderate. The "supersonic-radiative" scenario induces nearly no effects on the type 1b and type 2 PSC properties, compared to the "supersonic" case, and only a smaller increases in occurrence and surface areas of type 1a PSCs (compare upper and lower rows in Figures 14 and 15).

6. Conclusions.

Microphysical simulations using domain filling trajectories have been performed to investigate the influence on PSC properties of enhanced concentrations of HNO_3 and H_2O, caused by aircraft emissions in year 2015 scenarios. The results show that emissions from a projected fleet subsonic aircraft only cause minor influences on PSC occurrence and surface area densities. However, the effects from a combined fleet of subsonic and supersonic aircraft clearly show up in the simulations. Increased concentrations of HNO_3 and H_2O in the "supersonic" scenarios on the order of 5-10 % will have a direct influence on the thermodynamic threshold temperatures for the existence of NAT, STS, and ice in the NH polar stratosphere. This may cause the frequency of occurrence of temperatures below these thresholds to increase by 2-5% and give rise to increases in Type 1b PSC equilibrium volumes of about 10 %.

Performing more detailed microphysical simulations, which allow the inherent temperature hysteresis in the life cycles of different PSC particle types to be taken into account, using temperature histories from a large number of individual airparcels, the influences of the supersonic aircraft emissions become more pronounced. In particular, the increased concentrations of water vapour imply higher freezing temperatures for ice in STS Type 1b PSC particles, required for the formation of solid Type 1a and Type 2 PSCs. Both the frequencies of occurrence and the vortex-averaged surface area densities of solid type PSCs may increase by 50-100% in continuous periods throughout the winter. Although the surface areas of these types of PSCs are relatively small, compared to the much more abundant liquid Type 1b PSCs, only the solid type PSC could be responsible for significant denitrification and dehydration of the Arctic stratosphere. Detailed multi-level sedimentation calculations are not possible within a domain-filling trajectory approach. However, detailed calculations of the gravitational particle-fall-out of individual airparcels and model-level averages of exchange rates in HNO_3 and H_2O between layers can be made. These calculations show that the "supersonic" aircraft emission-induced formation of solid type PSC particles may increase the denitrification rate by about 38 % and even lead to larger relative increases in dehydration. It should be noticed that these conclusions depend on the winter chosen (1989/90) which was relatively cold.

Climate model calculations [*Shindell et al.*, 1998] have predicted that NH stratospheric December-January temperatures may decrease by 3-10 K in 2010-2019 due to increased concentrations of greenhouse gases, less frequent stratospheric warmings, and ozone depletion. For a rough comparison between possible "supersonic" aircraft effects and decreased stratospheric temperatures, the calculations on model level 5, using the University of Oslo "no-aircraft" concentrations of HNO_3 and H_2O, have been repeated with all temperatures lowered by 3 K. The results are shown in Figure 16. Quite obviously, the formation of solid type PSC is much more sensitive to this change in temperatures conditions, compared to the aircraft perturbations of H_2O, which only increase the frost point temperatures on the order of 0.2-0.4 K. However, both the possible decreasing stratospheric temperatures, due to increased greenhouse gases and ozone depletion, and the increasing frostpoint temperatures, due to supersonic aircraft emissions, work in the same direction, mainly affecting the solid type PSC formation, which may lead to increased denitrification and possible dehydration

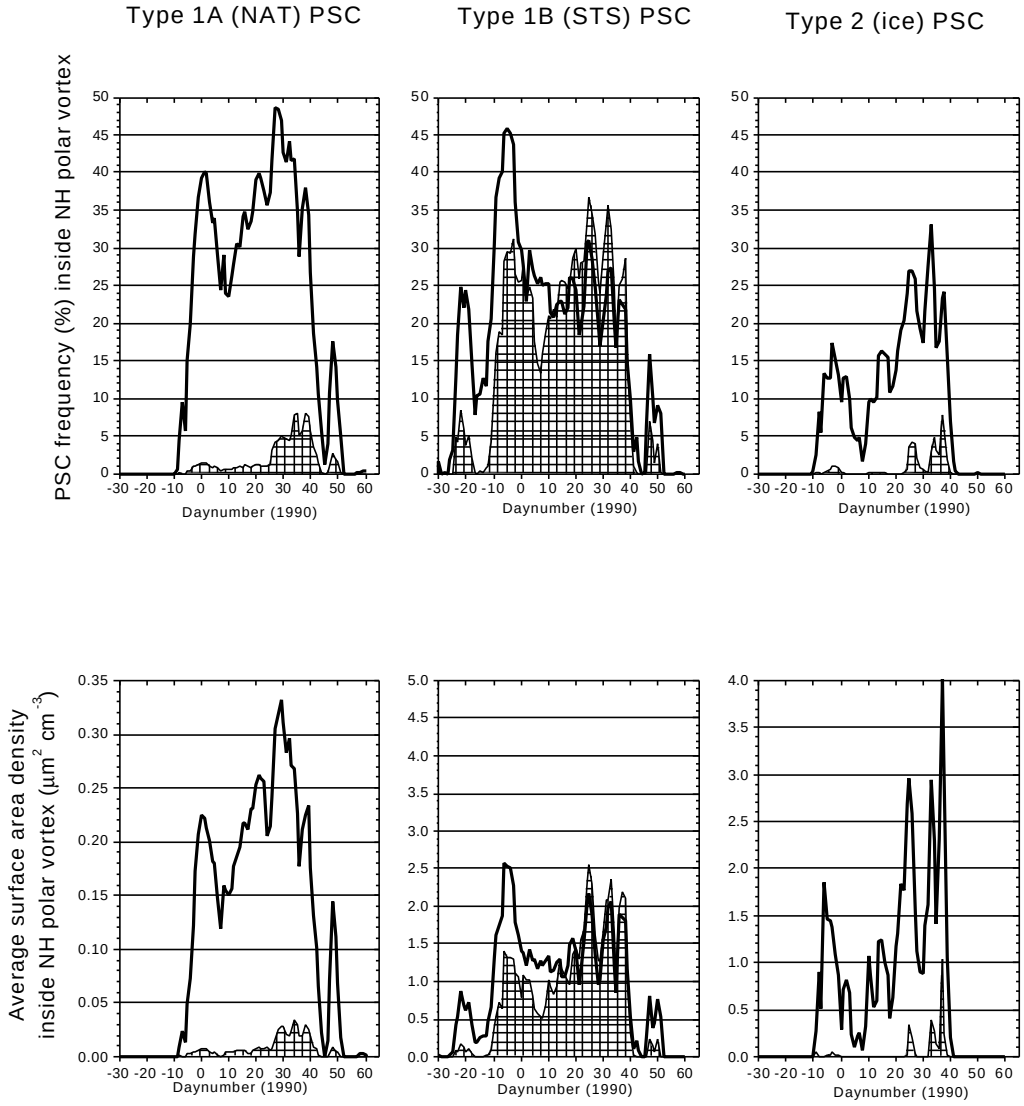

Figure 16 The upper row shows the frequency of occurrence of different types of PSC particles at model level 5, calculated using the University of Oslo 'no aircraft' concentrations of HNO_3 and H_2O (hatched curves, cf. Figure 11), compared to a 'no aircraft' simulation with all temperatures lowered by 3 K (thick curves). The lower row shows the calculated vortex-averaged surface area densities in the same two simulations (cf. Figure 12).

Acknowledgements.

This work has been performed within the EU project "Modelling of the impact on ozone and other chemical compounds in the atmosphere from airplane emissions" (AEROCHEM II, contract ENV4-CT97-0621, 1998-2000), funded by the European Commission Environment and Climate programme (4th Framework programme).

Ken Carslaw is acknowledged for provision of a computer code for calculations of equilibrium STS particle compositions and volumes.

References.

Baughcum, S. L., and Henderson, S. C. Aircraft Emission Scenarios Projected in Year 2015 for the NASA Technology Concept Aircraft (TCA) High Speed Civil Transport, *NASA-CR-1998-207635*, 1998.

Carslaw, K.S., B. Luo, and T. Peter, An analytic expression for the composition of aqueous HNO_3-H_2SO_4 stratospheric aerosols including gas phase removal of HNO_3, *Geophys Res. Lett. 22*, 1877-1880, 1995.

Chiou, E.W., M.P. McCormick, and W.P.Chu, Global water vapor distributions in the stratosphere and upper troposphere derived from 5.5 years of SAGE II observations (1986-1991), *J. Geophys. Res., 102*, 19105-19118, 1997.

Considine, D.B. et al., A polar stratospheric cloud parameterization for the global modelling initiative three dimensional model and its response to stratospheric aircraft, *J. Geophys. Res. 105*, 3955-3973, 2000.

Hitchman, M.H., M. McKay, and C.R. Trepte, A climatology of stratospheric aerosol, *J. Geophys. Res. 99*, 20689-20700, 1994.

Intergovernmental Panel on Climate Change (IPCC), Climate Change 1995, The Science of Climate Change, J.T. Houghton, L.G. Meira Filho, B.A. Callander, N. Harris, A. Kattenberg, and K. Maskell (Eds.), Cambridge Univ. Press, Cambridge, UK), 1995.

Intergovernmental Panel on Climate Change (IPCC), Aviation and the global atmosphere, Cambridge Univ. Press, Cambridge, UK, 1999.

Isaksen, I.S.A., Rognerud, B., Stordal, F., Coffey, M.T. and Mankin, W.G. Studies of Arctic stratospheric ozone in a 2-d model including some effects of zonal asymmetries. *Geophys. Res. Lett., 17*, 557-560., 1990.

Keating, G.M., M.C. Pitts, and D.F. Young, Ozone reference models for the middle atmosphere, *Adv. Space Res., 10*, 317-355, 1990.

Knudsen, B.M. and J.-U. Grooß, Northern midlatitude stratospheric ozone dilution in spring modeled with simulated mixing, *J. Geophys. Res., 105*, 6885-6890, 2000.

Kylling, A., Stamnes, K. and Tsay, S.-C. A reliable and efficient two-stream algorithm for spherical radiative transfer: Documentation of accuracy in realistic layered media, *J. Atm. Chem., 21*, 115-150., 1995.

Larsen, N., Chemical understanding of ozone loss - heterogeneous processes: Microphysical understanding and outstanding issues, Proceedings of the Fifth European Symposium on Polar Stratospheric Ozone Research, St. Jean de Luz, France, September 1999, *Air Pollution Research Report*, European Commission, 2000a.

Larsen, N., Polar Stratospheric Clouds, Microphysical and optical models, *DMI Scientific Report 00-06*, Danish Meteorological Institute, Copenhagen, 2000b.

Manney, G.L., R.W. Zurek, M.E. Gelman, A.J. Miller, and R. Nagatani, The anomalous Arctic lower stratospheric polar vortex of 1992-1993, *Geophys. Res. Lett. 21*, 2405-2408, 1994.

Manney, G.L., R.W. Zurek, L. Froideveaux, J.W. Waters, A. O'Neill, and R. Swinbank, Lagrangian transport calculations using UARS dat. Part II: Ozone, *J. Geophys. Res., 52*, 3069-3081, 1995.

Morcrette, J.-J., Radiation and cloud radiative properties in the ECMWF operational weather forecast model, *J. Geophys. Res., 96*, 9121-9132, 1991.

Morris, G.A. et al., Trajectory mapping and applications to data from the Upper Atmosphere Research Satellite, *J. Geophys. Res., 100*, 16,491-16,505, 1995.

Pawson, S., B. Naujokat, and K. Labitzke, On the polar stratospheric cloud formation potential of the northern stratosphere, *J. Geophys. Res. 100*, 23215-23225, 1995.

Peter, Th, C. Brühl and P.J. Crutzen, Increase in the PSC-formation Probability Caused by High-flying Aircraft, *Geophys. Res. Lett. 18*, 1465-1468, 1991.

Pitari, G., V. Rizi, L. Ricciardulli, and G. Visconti, High-Speed Civil Transport Impact: Role of sulphate, nitric acid trihydrate, and ice aerosols studied with a two-dimensional model including aerosol physics, *J. Geophys Res. 98*, 23141-23164, 1993.

Prather, M., Numerical advection by conservation of second-order moments. *J. Geophys. Res., 91*, 6671-6681, 1986.

Prather, M., McElroy, M., Wolfsy, S., Russell, G., and Rind, D. Chemistry of the global troposphere: Fluorocarbons as tracers of air motion, *J. Geophys. Res., 92*, 6579-6613., 1987.

Prather, M., Garcia, M.M., Suozzo, R., and Rind, D., Global impact of the Antarctic ozone hole: Dynamical dilution with a three-dimensional chemical transport model, *J. Geophys. Res. 95*, 3449-3471, 1990.

Rind, D., Suozzo, R., Balachandran, N. K., Lacis, A. and Russell, G., The GISS Global Climate-Middle Atmosphere Model. Part I: Model Structure and Climatology. *J. Atm. Sci., 45*, 329-370, 1988.

Rummukainen, M., Modeling stratospheric chemistry in a global three-dimensional chemical transport model, SCTM-1. Model development. *Finnish Meteorological Institute Contributions*, No. 19, 1996.

Rummukainen, M., Isaksen, I.S.A., Rognerud, B., and Stordal, F., A global model tool for three-dimensional multiyear stratospheric chemistry simulations: Model description and first results. *J. Geophys. Res., 104*, 26437-26456, 1999.

Shindell, D.T., D.Rind, and P. Lonergan, Increased polar stratospheric ozone losses and delayed eventual recovery owing to increasing greenhouse-gas concentrations, *Nature 392*, 589-592, 1998.

Stordal, F., Isaksen, I.S.A. and Horntvedt, K., A diabatic circulation two-dimensional model with photochemistry: Simulations of ozone and long-lived tracers with surface sources. *J. Geophys. Res., 90*, 5757-5776, 1985.

World Meteorological Organization (WMO), Scientific assessment of ozone depletion: 1998, *Rep. 44, Global Ozone Res. and Monit. Proj.*, Geneva, 1999.

DANISH METEOROLOGICAL INSTITUTE

Scientific Reports

Scientific reports from the Danish Meteorological Institute cover a variety of geophysical fields, i.e. meteorology (including climatology), oceanography, subjects on air and sea pollution, geomagnetism, solar-terrestrial physics, and physics of the middle and upper atmosphere.

Reports in the series within the last five years:

No. 95-1
Peter Stauning and T.J. Rosenberg: High-Latitude, day-time absorption spike events 1. morphology and occurrence statistics
Not published

No. 95-2
Niels Larsen: Modelling of changes in stratospheric ozone and other trace gases due to the emission changes : CEC Environment Program Contract No. EV5V-CT92-0079. Contribution to the final report

No. 95-3
Niels Larsen, Bjørn Knudsen, Paul Eriksen, Ib Steen Mikkelsen, Signe Bech Andersen and Torben Stockflet Jørgensen: Investigations of ozone, aerosols, and clouds in the arctic stratosphere : CEC Environment Program Contract No. EV5V-CT92-0074. Contribution to the final report

No. 95-4
Per Høeg and Stig Syndergaard: Study of the derivation of atmospheric properties using radio-occultation technique

No. 95-5
Xiao-Ding Yu, **Xiang-Yu Huang** and **Leif Laursen** and Erik Rasmussen: Application of the HIRLAM system in China: heavy rain forecast experiments in Yangtze River Region

No. 95-6
Bent Hansen Sass: A numerical forecasting system for the prediction of slippery roads

No. 95-7
Per Høeg: Proceeding of URSI International Conference, Working Group AFG1 Copenhagen, June 1995. Atmospheric research and applications using observations based on the GPS/GLONASS System, Not published

No. 95-8
Julie D. Pietrzak: A comparison of advection schemes for ocean modelling

No. 96-1
Poul Frich (co-ordinator), H. Alexandersson, J. Ashcroft, B. Dahlström, G.R. Demarée, A. Drebs, A.F.V. van Engelen, E.J. Førland, I. Hanssen-Bauer, R. Heino, T. Jónsson, K. Jonasson, L. Keegan, P.Ø. Nordli, **T. Schmith**, **P. Steffensen**, H. Tuomenvirta, O.E. Tveito: North Atlantic Climatological Dataset (NACD Version 1) - Final report

No. 96-2
Georg Kjærgaard Andreasen: Daily response of high-latitude current systems to solar wind variations: application of robust multiple regression. Methods on Godhavn magnetometer data

No. 96-3
Jacob Woge Nielsen, Karsten Bolding Kristensen, Lonny Hansen: Extreme sea level highs: a statistical tide gauge data study

No. 96-4
Jens Hesselbjerg Christensen, Ole Bøssing Christensen, Philippe Lopez, Erik van Meijgaard, Michael Botzet: The HIRLAM4 Regional Atmospheric Climate Model

No. 96-5
Xiang-Yu Huang: Horizontal diffusion and filtering in a mesoscale numerical weather prediction model

No. 96-6
Henrik Svensmark and Eigil Friis-Christensen: Variation of cosmic ray flux and global cloud coverage - a missing link in solar-climate relationships

No. 96-7
Jens Havskov Sørensen and Christian Ødum Jensen: A computer system for the management of epidemiological data and prediction of risk and economic consequences during outbreaks of foot-and-mouth disease. CEC AIR Programme. Contract No. AIR3 - CT92-0652

No. 96-8
Jens Havskov Sørensen: Quasi-automatic of input for LINCOM and RIMPUFF, and output conversion. CEC AIR Programme. Contract No. AIR3 - CT92-0652

No. 96-9
Rashpal S. Gill and Hans H. Valeur: Evaluation of the radarsat imagery for the operational mapping of sea ice around Greenland

No. 96-10
Jens Hesselbjerg Christensen, Bennert Machenhauer, Richard G. Jones, Christoph Schär, Paolo Michele Ruti, Manuel Castro and Guido Visconti: Validation of present-day regional climate simulations over Europe: LAM simulations with observed boundary conditions

No. 96-11
Niels Larsen, Bjørn Knudsen, Paul Eriksen, Ib Steen Mikkelsen, Signe Bech Andersen and Torben Stockflet Jørgensen: European Stratospheric Monitoring Stations in the Artic: An European contribution to the Network for Detection of Stratospheric Change (NDSC): CEC Environment Programme Contract EV5V-CT93-0333: DMI contribution to the final report

No. 96-12
Niels Larsen: Effects of heterogeneous chemistry on the composition of the stratosphere: CEC Environment Programme Contract EV5V-CT93-0349: DMI contribution to the final report

No. 97-1
E. Friis Christensen og C. Skøtt: Contributions from the International Science Team. The Ørsted Mission - a pre-launch compendium

No. 97-2
Alix Rasmussen, Sissi Kiilsholm, Jens Havskov Sørensen, Ib Steen Mikkelsen: Analysis of tropospheric ozone measurements in Greenland: Contract No. EV5V-CT93-0318 (DG 12 DTEE): DMI's contribution to CEC Final Report Arctic Trophospheric Ozone Chemistry ARCTOC

No. 97-3
Peter Thejll: A search for effects of external events on terrestrial atmospheric pressure: cosmic rays

No. 97-4
Peter Thejll: A search for effects of external events on terrestrial atmospheric pressure: sector boundary crossings

No. 97-5
Knud Lassen: Twentieth century retreat of sea-ice in the Greenland Sea

No. 98-1
Niels Woetman Nielsen, Bjarne Amstrup, Jess U. Jørgensen:
HIRLAM 2.5 parallel tests at DMI: sensitivity to type of schemes for turbulence, moist processes and advection

No. 98-2
Per Høeg, Georg Bergeton Larsen, Hans-Henrik Benzon, Stig Syndergaard, Mette Dahl Mortensen: The GPSOS project
Algorithm functional design and analysis of ionosphere, stratosphere and troposphere observations

No. 98-3
Mette Dahl Mortensen, Per Høeg:
Satellite atmosphere profiling retrieval in a nonlinear troposphere
Previously entitled: Limitations induced by Multipath

No. 98-4
Mette Dahl Mortensen, Per Høeg:
Resolution properties in atmospheric profiling with GPS

No. 98-5
R.S. Gill and M. K. Rosengren
Evaluation of the Radarsat imagery for the operational mapping of sea ice around Greenland in 1997

No. 98-6
R.S. Gill, H.H. Valeur, P. Nielsen and K.Q. Hansen: Using ERS SAR images in the operational mapping of sea ice in the Greenland waters: final report for ESA-ESRIN's: pilot projekt no. PP2.PP2.DK2 and 2nd announcement

of opportunity for the exploitation of ERS data projekt No. AO2..DK 102

No. 98-7
Per Høeg et al.: GPS Atmosphere profiling methods and error assessments

No. 98-8
H. Svensmark, N. Woetmann Nielsen and A.M. Sempreviva: Large scale soft and hard turbulent states of the atmosphere

No. 98-9
Philippe Lopez, Eigil Kaas and Annette Guldberg: The full particle-in-cell advection scheme in spherical geometry

No. 98-10
H. Svensmark: Influence of cosmic rays on earth's climate

No. 98-11
Peter Thejll and Henrik Svensmark: Notes on the method of normalized multivariate regression

No. 98-12
K. Lassen: Extent of sea ice in the Greenland Sea 1877-1997: an extension of DMI Scientific Report 97-5

No. 98-13
Niels Larsen, Alberto Adriani and Guido DiDonfrancesco: Microphysical analysis of polar stratospheric clouds observed by lidar at McMurdo, Antarctica

No.98-14
Mette Dahl Mortensen: The back-propagation method for inversion of radio occultation data

No. 98-15
Xiang-Yu Huang: Variational analysis using spatial filters

No. 99-1
Henrik Feddersen: Project on prediction of climate variations on seasonel to interannual timescales (PROVOST) EU contract ENVA4-CT95-0109: DMI contribution to the final report:Statistical analysis and post-processing of uncoupled PROVOST simulations

No. 99-2
Wilhelm May: A time-slice experiment with the ECHAM4 A-GCM at high resolution: the experimental design and the assessment of climate change as compared to a greenhouse gas experiment with ECHAM4/OPYC at low resolution

No. 99-3
Niels Larsen et al.: European stratospheric monitoring stations in the Artic II: CEC Environment and Climate Programme Contract ENV4-CT95-0136. DMI Contributions to the project

No. 99-4
Alexander Baklanov: Parameterisation of the deposition processes and radioactive decay: a review and some preliminary results with the DERMA model

No. 99-5
Mette Dahl Mortensen: Non-linear high resolution inversion of radio occultation data

No. 99-6
Stig Syndergaard: Retrieval analysis and methodologies in atmospheric limb sounding using the GNSS radio occultation technique

No. 99-7
Jun She, Jacob Woge Nielsen: Operational wave forecasts over the Baltic and North Sea

No. 99-8
Henrik Feddersen: Monthly temperature forecasts for Denmark - statistical or dynamical?

No. 99-9
P. Thejll, K. Lassen: Solar forcing of the Northern hemisphere air temperature: new data

No. 99-10
Torben Stockflet Jørgensen, Aksel Walløe Hansen: Comment on "Variation of cosmic ray flux and global coverage - a missing link in solar-climate relationships" by Henrik Svensmark and Eigil Friis-Christensen

No. 99-11
Mette Dahl Meincke: Inversion methods for atmospheric profiling with GPS occultations

No. 99-12
Benzon, Hans-Henrik; Olsen, Laust: Simulations of current density measurements with a Faraday Current Meter and a magnetometer

No. 00-01
Høeg, P.; Leppelmeier, G: ACE: Atmosphere Climate Experiment: proposers of the mission

No. 00-02
Høeg, P.: FACE-IT: Field-Aligned Current Experiment in the Ionosphere and Thermosphere

No. 00-03
Allan Gross: Surface ozone and tropospheric chemistry with applications to regional air quality modeling. PhD thesis

No. 00-04
Henrik Vedel: Conversion of WGS84 geometric heights to NWP model HIRLAM geopotential heights

No. 00-05
Jérôme Chenevez: Advection experiments with DMI-Hirlam-Tracer
(In Press)

No. 00-06
Niels Larsen: Polar stratospheric clouds micro-physical and optical models

No. 00-07
Alix Rasmussen: "Uncertainty of meteorological parameters from DMI-HIRLAM"
(In Press)

No. 00-08
A.L. Morozova: Solar activity and Earth's weather. Effect of the forced atmospheric transparency changes on the troposphere temperature profile studied with atmospheric models
(In Press)